

Online Condition Monitoring of MV Switchgear Using *D*-Dot Sensor to Predict Arc-Faults

Ghulam Amjad Hussain, *Member, IEEE*, Muhammad Shafiq, Matti Lehtonen, *Member, IEEE*, and Murtaza Hashmi

Abstract—High energy arc faults in medium-voltage (MV) switchgear are serious hazards to personnel or equipment, and may cause process interruptions. Most of the electrical faults leading to arc are developed slowly, e.g., due to insulation degradation or bad connection. In this paper, the detection of partial discharges (PDs) and low energy arcing between loose contacts has been proposed for online monitoring of MV switchgear. The PD measurements in a switchgear panel and arcing measurements across a 0.2-mm sphere-to-rod gap have been carried out. Measured signals are captured by a differential electric field sensor (*D*-dot sensor) and recorded by a high-frequency oscilloscope. In general, online measured signals are suppressed by high-frequency noise, and therefore, de-noising of measurements is of paramount importance to get reliable information about a fault. An implementation of discrete wavelet transform, to de-noise the measured signals, has been proposed in this paper. Comparison with a well-known infinite impulse response filtering technique has been made. Time and frequency domain comparisons between original and de-noised signals reveal the significance of this technique for arc fault prediction in MV switchgear. A layout for the integration of online monitoring to central control is also presented.

Index Terms—Arc discharge, differential electric field sensor, distribution automation, online condition monitoring, partial discharge, signal de-noising, switchgear, wavelet transform.

I. INTRODUCTION

BAD connections and insulation degradation are the two major causes of high energy arc faults in switchgear, that are developed slowly [1]. This results in catastrophic damages to the equipment and the personnel working in the vicinity. According to [2], a case study was performed which showed that 60-80% of all arcing events occurred in the switchgear were caused by faulty connections. The mechanism of how a faulty connection develops and ultimately leads to an arcing fault is well described in [2]–[4]. The energy of such faults is dependent on the magnitude of voltage, current and arc duration [5], [6]. Degradation of insulation materials

is another main reason for arc faults. The lifetime of an electrical insulation depends on the thermal, electrical, ambient and mechanical (TEAM) stresses [7], [8]. Electrical stresses such as overvoltages and PD activity are frequent causes of insulation degradation among all of the above [9], [10]. A major portion of arc faults is still due to accidental contacts such as slippage of tools and animals (lizards, rats, etc). Some precautionary measures, such as use of insulated bus bars, training and education of workers and improved procedures for maintenance can help to reduce the happening of arc flash due to accidental contacts [4].

PDs and low energy arcing faults between loose contacts inside the air-insulated switchgear are sources of discharge transient signals (high frequency current pulses) and other physical emissions such as electromagnetic (EM), acoustic and ultraviolet. Due to small rise time, the spectrum of EM radiations is in radio frequency region [11], [12]. The propagation of EM waves depends on the frequency spectrum. These emissions can be detected and measured by various radio frequency sensors suitable for a certain application. The sensors that measure physical phenomenon non-intrusively, such as EM signals, acoustic emissions or ultraviolet light, are called unconventional sensors. On the contrary, conventional sensors are used in contact with the high voltage (HV) parts and are mostly measuring current or voltage.

Due to switch-over from periodic maintenance to condition based maintenance, online monitoring concept has become more popular for the last two decades. In this research a differential electric field sensor (a monopole antenna of much smaller size) has been developed and used for transient detection. It has not been used for transient detection in air insulated switchgear so far, hence it is a unique application of this sensor. Existing application of this sensor are explained below.

In early 90s open ended coaxial type connector was used as a sensor for permittivity or dielectric measurement of biological substances [13], [14]. These sensors are similar to the *D*-dot sensor in construction and operating principle. In these applications, the open ended line is inserted into the sample and power flows from the generator towards the open end where it is reflected back towards the generator. An input reflection coefficient (or input admittance) is measured at a specific frequency and temperature. Then reflection coefficient data is related to the dielectric properties of the sample. The analysis of dielectric properties of damaged biological tissues in comparison with the healthy tissues assists in diagnostics

Manuscript received July 1, 2015; accepted August 24, 2015. Date of publication August 27, 2015; date of current version October 15, 2015. This work was supported in part by the School of Electrical Engineering, Aalto-yliopisto, Espoo, Finland, and in part by the Finnish Foundation for Technology Promotion. The associate editor coordinating the review of this paper and approving it for publication was Dr. E.-H. Yang.

G. A. Hussain, M. Shafiq, and M. Lehtonen are with the School of Electrical Engineering, Aalto University, Aalto FI-00076, Finland (e-mail: amjad.hussain@aalto.fi; muhammad.shafiq@aalto.fi; matti.lehtonen@aalto.fi).

M. Hashmi is with Saudi Aramco, Dhahran 31311, Saudi Arabia (e-mail: ghulam.hashmi@aramco.com).

Color versions of one or more of the figures in this paper are available online at <http://ieeexplore.ieee.org>.

Digital Object Identifier 10.1109/JSEN.2015.2474122

of fatal diseases such as cancer and determines the need of operation or suitable therapy.

Unlike the above studies where the effect of dielectrics on the reflection coefficient when the open end of coaxial cable is inserted into a sample and the power flowing from the generator towards the open end from where it is reflected back towards the generator is analyzed, Burkhart [15] introduced a new application of the sensor for the measurement of power and frequency of the microwave energy in a cavity or waveguide by coupling it into the open end to a matched termination. An open ended semi-rigid coaxial cable was characterized for use as a coupling element for the measurement of high power microwaves. The sensor inserted no more than flush with the inner waveguide wall, is a convenient way to couple out a sample of the power. The sensor is inserted into the waveguide in a direction parallel to the electric field.

A similar application of *D*-dot sensor is reported in [16] and [17] for near electric field measurement systems for planar microwave circuits due to its high bandwidth, miniature size and ease of installation in microwave circuits. In these applications, modified versions of the sensor are used by attaching a micro-strip to the centre conductor of the sensor.

Andrews [18] reports the application of *D*-dot sensor as a short monopole antenna for the transmission (send and receive) ultra wide band (UWB) communication signals. In [19], the *D*-dot sensor is proposed for the measurement of fast-front high voltages, e.g. the residual voltage of surge arrestors. The fast-front voltages or currents are normally generated by system faults or disconnecter operation within gas insulated switchgear (GIS), operation of surge arrestors or puncture of insulators etc. The probe consists of three identical copper toroids placed around a high voltage electrode and all are coaxially assembled in a large earthed cylinder. Hence, the sensor designed for this application is different in construction to the above applications.

In [20], *D*-dot sensor is installed as flush mounted in a sulfur hexafluoride container having conical to plane gap. The picoseconds flashovers are generated by applying high voltage across the electrodes of the chamber. The collapsed voltage is measured by the *D*-dot sensors. This *D*-dot sensor is similar to the one introduced in this paper except the centre conductor is kept uncut in our research for better sensitivity.

Various types of commercially available coaxial connectors (*D*-dot sensors) are tested and compared by measuring nanosecond high voltage pulses generated by an electromagnetic pulse (EMP) simulator in [21]. The EMP simulator is a parallel plate transmission line connected to a high voltage pulse generator capable of producing 2-5 ns rise times and voltages up to 100 kV. Despite the largely diverse characteristics of the sensors, their outputs are rather consistent, indicating that all of the selected sensors are equally capable of measuring ns-range pulses.

The following sections explain the construction, working principle and performance of the sensor. Performance is evaluated using experimental setup in the laboratory. The major problem with online condition monitoring is the interference of external airborne noise. Hence, de-noising is of paramount importance, in order to extract useful features to make

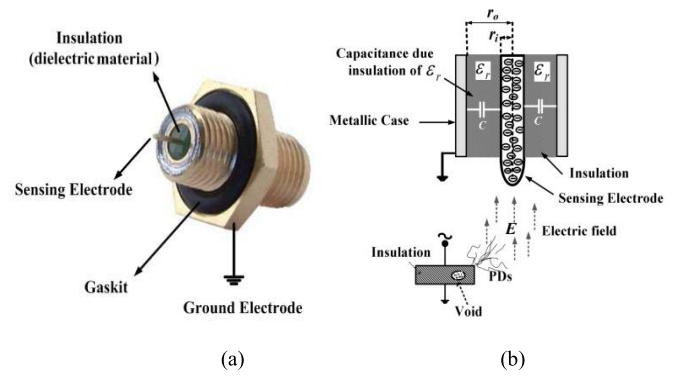


Fig. 1. (a) Sensor head. (b) Working principle.

correct decision. This paper provides an efficient de-noising technique based on Discrete Wavelet Transform (DWT). Significance of the proposed technique has been proved with the help of comparisons between the captured and de-noised signals with DWT and infinite impulse response (IIR). Integration of *D*-dot sensor to the supervisory control and automation system provides comprehensive protection and monitoring of switchgear.

II. CONSTRUCTION AND WORKING PRINCIPLE OF *D*-DOT SENSOR

The *D*-dot sensor is a differential electric field probe. It is a co-axial sensor made from a standard straight bulkhead subminiature version 'A' (SMA) connector/ jack. Fig. 1(a) shows the sensor's head. Outer case works as a ground electrode and the centre conductor serves as a sensing electrode. The two electrodes are separated by Teflon (PTFE) insulation material. The whole sensor thus makes a coaxial (cylindrical) assembly.

The working principle, elaborated in Fig. 1(b), is similar to a monopole antenna. The electric field, produced by discharge transients, generates a surface charge density on the sensing electrode (centre conductor) of the co-axial sensor. At zero frequency (direct current), the sensing electrode is held at zero potential through the 50Ω terminating resistance. When the electric field (E) varies, the charge varies linearly. *D*-dot probes effectively measure the time derivative of the electric flux density at the surface of the sensing electrode [18]. This is equivalent to the measurement of the time rate of change of the surface charge density or displacement current density i.e. $J_D = dD/dt = \dot{D}$ [19]. The electric flux density D is related to the electric field intensity E by the expression $D = \epsilon_0 E$, where ϵ_0 is the permittivity of free space.

As *D*-dot sensor is a capacitive sensor, hence the output current of the sensor can be represented as,

$$i(t) = C \frac{dV(t)}{dt} \quad (1)$$

where C is the cumulative capacitance between the discharge source and the centre conductor of the sensor head and also the capacitance of the measurement system [22]. Electric potential and electric field are related to each other as $V(t) = \rho E(t)$,



Fig. 2. *D*-dot sensor mounted on a grounded plane.

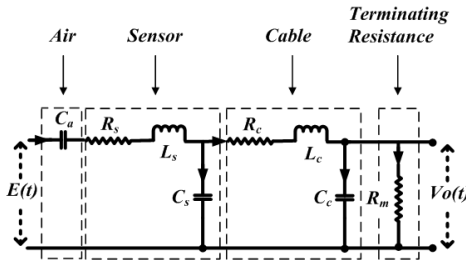


Fig. 3. Equivalent circuit of the *D*-dot sensor.

where p is the distance from the discharge source to the sensor's head. Hence, (1) can be written as,

$$i(t) = pC \frac{dE(t)}{dt} \quad (2)$$

A standard SMA connector with a 4.4 mm long centre conductor (protruding above the ground plane) has a cut-off frequency of 18 GHz. Decreasing the length of the centre conductor will increase its bandwidth but reduce its sensitivity [18]. Fig. 2 shows a *D*-dot sensor, installed on a ground plane, used for the measurements in the laboratory.

The equivalent circuit of the *D*-dot sensor is shown in Fig. 3. It mainly consists of series and parallel capacitances [22], [23]. The following sub-sections explain the procedure to determine these circuit parameters.

A. Determination of Sensor's Capacitance

The capacitance of sensor's head, represented by C_s , is the cumulative capacitance between the sensing electrode (centre conductor of the sensor) and the grounded metallic casing of the sensor as shown in Fig. 1(b). It can be calculated by the formula for the cylindrical capacitor given by,

$$C_s = l_s \frac{2\pi k_s \epsilon_0}{\ln \left[\frac{r_o}{r_i} \right]} \quad (3)$$

where l_s is the length of the sensor, r_i is the radius of sensing electrode, r_o is the distance between the centre of sensing electrode and the metallic case, and k_s is the relative dielectric constant of insulation material (usually PTFE). Both the radii r_i and r_o are marked in Fig. 1(b).

B. Determination of Sensor's Resistance

The resistance of the sensor R_s is the resistance of centre conductor of the sensor which can be measured by using Ohm meter.

C. Determination of Sensor's Inductance

The inductance of the sensor L_s is very negligible. However, it can be calculated by using the formula for a cylindrical object given by,

$$L_s = l_s \frac{\mu_o \mu_{rs}}{2\pi} \ln \left[\frac{r_o}{r_i} \right] \quad (4)$$

where μ_o is the permeability of air and μ_{rs} is the relative permeability of dielectric material of sensor.

D. Determination of Air Capacitance or Series Capacitance

Air capacitance or series capacitance (C_a) comprises of the capacitance of air between the source of electric field and its sensing electrode. It is hard to be calculated but can be measured from an installed setup using the procedure given below. The same methodology is introduced by the authors for Rogowski coil sensor in [23], which proved to be practically successful in determining the model parameters. The resonant frequency of the whole measurement system can be given as:

$$f = \frac{1}{2\pi \sqrt{LC}} \quad (5)$$

where L and C are the equivalent inductance and capacitance of the measurement system including sensor and signal transmission cable. In order to find the resonant frequency of the sensor, a PD pulse signal from a signal generator is injected into the test object and output signal is measured by the sensor. Resonant frequency of the measurement system given by (5), is calculated through fast Fourier transform (FFT) of the signal.

Now, a known capacitance (C_1) is then connected at the terminal of the sensor, before connecting the sensor to the coaxial transmission cable and the same PD pulse is injected. The new resonant frequency is based on L and $C + C_1$ in this case as,

$$f_1 = \frac{1}{2\pi \sqrt{L(C + C_1)}} \quad (6)$$

The value of equivalent capacitance can be calculated by dividing the equation (5) by (6),

$$\frac{f}{f_1} = \frac{C}{C + C_1} \quad (7)$$

In (7), f , f_1 and C_1 are known, hence C can be calculated. Whereas, $C = C_a + C_s + C_c$. C_s and C_c are calculated as explained in sub-sections (A) and (G). Ultimately, C_a is determined by subtracting the values of C_s and C_c .

E. Determination of Cable's Resistance

The cable resistance can be measured by using Ohm meter or can be given in its datasheet. A typical value of standard measurement purpose coaxial cable is 50 Ohms.

F. Determination of Cable's Inductance

Inductance per unit length of the coaxial cable can be determined by the following formula,

$$\frac{L_c}{l_c} = \frac{\mu_o \mu_{rc}}{2\pi} \ln \left[\frac{r_{oc}}{r_{ic}} \right] \quad (8)$$

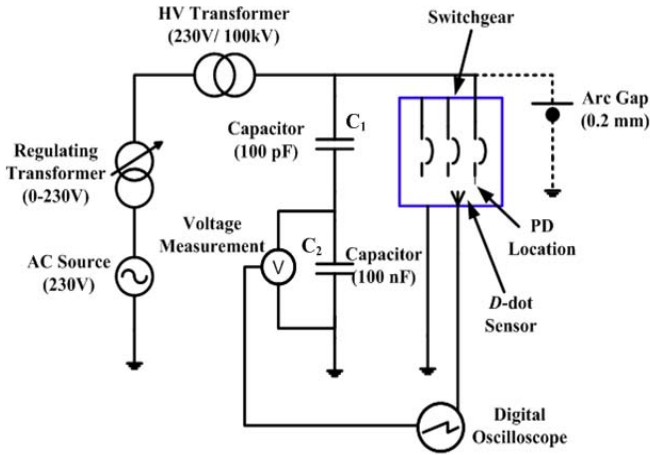


Fig. 4. Measurement setup (dotted section shows arcing setup).

where l_c is the length of the cable, μ_o is the permeability of air, r_{ic} is the radius of the centre conductor of coaxial cable, r_{oc} is its external radius of the whole cable and μ_{rc} is the relative permeability of dielectric material of coaxial cable.

G. Determination of Cable's Capacitance

The capacitance of cable (C_c) can also be measured by using the formula for cylindrical capacitor. It is the capacitance between the centre conductor and the outer casing of the cable. Capacitance per unit length of the coaxial cable can be calculated by,

$$\frac{C_c}{l_c} = \frac{2\pi k_c \epsilon_o}{\ln \left[\frac{r_{oc}}{r_{ic}} \right]} \quad (9)$$

where k_c is the relative dielectric constant of cable insulation material.

III. PERFORMANCE OF *D*-DOT SENSOR

A. Experimental Setup and Data Acquisition

The measurement setup was arranged in the laboratory to measure two types of discharges, i.e. PD and Arcing, being the two incipient defects in switchgear which may lead to high energy arc faults. PD source was installed inside the switchgear whereas the arcing measurements were done with a sphere-to-rod gap assembly having 0.2 mm arc gap as shown in Figure 4. Dotted lines are shown to replace the switchgear panel with arc gap.

For PD measurement, circuit breaker of the switchgear was put in the closed position and the outgoing side of one phase was open circuited while other two were grounded. Open ended phase was energized and used to study partial discharge. PD source (an epoxy-resin solid insulator with air bubble) was installed at one phase by connecting its one side to the breaker terminal and other side to the ground. The metallic case of switchgear panel was grounded. *D*-dot sensor was installed in the switchgear compartment by fixing its ground plane to the metallic wall. Fig. 5 shows the physical location of *D*-dot sensor and PD source.

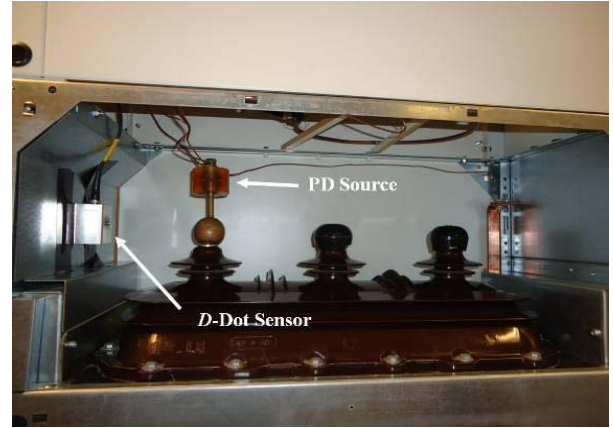


Fig. 5. Physical location of *D*-dot sensor & PD source in the switchgear compartment.

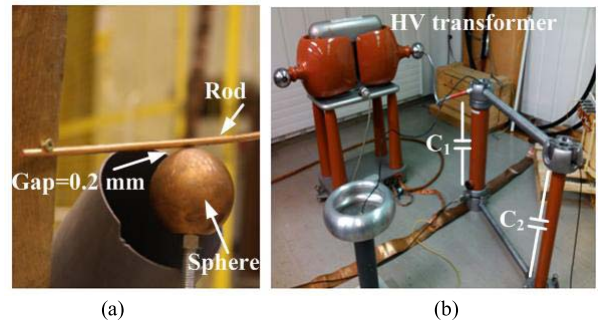


Fig. 6. (a) Sphere-to-rod assembly for arcing measurement (b) HV transformer and capacitive divider circuit.

Fig. 6(a) shows the 0.2 mm sphere-to-rod assembly which causes arcing discharges at 620 volts and Fig. 6 (b) shows HV transformer used in measurement and capacitive divider circuit for the measurement of applied voltage. The distance of the *D*-dot sensor from the PD source location was 24 cm and from arcing source 85 cm.

Signals were captured by *D*-dot sensor and recorded by oscilloscope at a sampling frequency of 2 GS/s and 20 GS/s for the PD and arcing faults respectively. The value of terminating resistance at the data acquisition port of oscilloscope was 50 ohms. Captured signals are shown in next sections.

B. Calibration and Performance of the Sensor

Most of the unconventional sensors discussed in [4], [24], and [25] are expensive due to their various technical requirements. For instance, high frequency current transformer (HFCT) is costly due to its insulation and low inductance design for high frequency applications. In addition, their designs are complicated and also require reasonable space for installation, whereas, *D*-dot sensor is an inexpensive sensor. It is simple in construction, smaller in size and can be installed inside the switchgear compartment easily. It has relatively higher bandwidth (up to 18GHz) which makes this sensor sensitive enough for most of the discharges [12].

According to IEC60270 standard, the calibration of sensors is done in such a way that a known short duration current pulse

TABLE I
OUTPUT AMPLITUDE COMPARISON BETWEEN
D-DOT SENSOR AND HFCT

Sensors	52 pC		100 pC	
	V _{PP} (mV)	V _P (mV)	V _{PP} (mV)	V _P (mV)
HFCT	15.5470	9.5157	32.7753	19.7012
<i>D</i> -dot Sensor	3.0115	1.4746	6.3448	3.1699
Pulse Transformer	-	24.3131	-	51.0477

*V_{PP} stands for peak to peak values of output signal whereas V_P stands for maximum value either in positive or negative side.

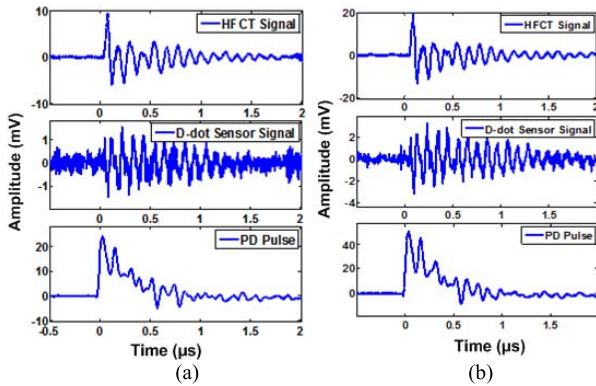


Fig. 7. Output of *D*-dot sensor. (a) Signals at 52 pC. (b) Signals at 100 pC.

(similar to PD pulse) is injected into a test object and output amplitude of sensor is scaled accordingly. Such calibration is valid for induction sensors (HFCT, Rogowski coil) or sensors in contact with HV part e.g. coupling capacitors (CC). It is possible to calibrate *D*-dot sensor for certain conditions only because air capacitance (C_a), shown in Fig. 3, can be variable. In our laboratory measurements, the distance between the PD source and the sensor was fixed. *D*-dot sensor was calibrated w.r.t a pre-calibrated HFCT. The calibration scales can be found in Table 1. In Fig. 7 and Table 1, the sensitivity of *D*-dot has been compared with HFCT for PD values of 52pC and 100pC. It is well known that the attenuation of electric field through air is very high as compared to the conductors. As the *D*-dot sensor measures air-borne differential electric field, the output of the sensor has lesser amplitude as compared to HFCT.

It has been reported in [25] that desired sensitivity range for PD measurements in air insulated cubicles is 10-100 pC. *D*-dot sensor is capable of detecting small level of discharges up to around 50 pC. However, the sensitivity of the sensor can further be increased by extending the length of centre conductor outward. Moreover due to wide bandwidth of *D*-dot sensor, it is likely that it may capture other high frequency electromagnetic disturbances. Such disturbance is prominent at lower PD levels (e.g. at 50 pC). Detailed technical comparison between *D*-dot sensor and HFCT can be found in [26]. *D*-dot sensor is immune to the external discharges because the external electric fields outside the closed switchgear panel are grounded through metallic sheets. There are only few places, e.g bushings, CTs, PTs, cable

terminations etc, which are prone to such fault and can be further inspected. Moreover cross-correlation techniques by using multiple sensors can help to find the exact location inside a panel. Due to all these factors, *D*-dot sensor has been found reliable for switchgear applications.

C. Challenges During Online Measurements

In spite of having a number of advantages, there are certain challenges to implement online monitoring. In case of periodic maintenance, the measurements are mostly done in shielded laboratories with filtered power supply where the effect of external noise is negligible. On contrary, the online testing and capacitive sensors have faced huge amount of external noise in the measured signals. Extracting the useful low-level signals from noisy backgrounds is a major challenge for online condition monitoring. In general, noise sources may be divided into the following [27]–[29]:

- Discrete Spectral Interference (DSI)
- Periodical pulses
- Random pulses
- White noise

DSI is a narrow-band interference caused by radio broadcasts (AM/FM) and communication networks and centered at certain dominant frequency. The dedicated frequency bands lie between few kHz to some tens of MHz (110 MHz). It can be eliminated by band stop filtering. Periodical pulse shaped disturbances are due to power electronic equipments and can be removed by gating circuits. This is relatively low frequency noise (in the range of some tens of kHz). Random pulses are caused by lightning or switching operations, whereas white noise is broadband interference caused by the measuring system itself [27]–[29]. White noise lies in the frequency range of HF to VHF and UHF (from 30MHz to 10 GHz) [12]. It is very difficult to get rid of these last two types of noises because of their similarity to discharge pulses especially when signal to noise ratio (SNR) is low [28]. With the advancement in digital signal processing (DSP) techniques, various methods for processing of high frequency transient signals have been reported during the last few years. Popular methods are finite impulse response (FIR) filters, infinite impulse response (IIR) filters, adaptive filtering and wavelet transform (WT) analysis [29], [30].

The measurements conducted in the HV laboratory are also affected by some of the above disturbances. Due to high bandwidth of *D*-dot sensor, it is likely that these high frequency noises may also be captured by it (can be noticed in Fig. 7). This makes the interpretation and analysis of signal as well as identification of nature of fault bit more difficult. DWT technique has been implemented for de-noising and pulse recognition in order to extract the useful information from the captured signals. Some typical onsite disturbances have been simulated and added to the signals captured in the laboratory and are de-noised by DWT also.

IV. De-NOISING OF DISCHARGE TRANSIENT SIGNALS

A. De-Noising Procedure Based on DWT

The basic theory of WT is explained in [30]. This section presents the de-noising procedure based on DWT. The steps

of the DWT procedure are stated below:

- A suitable mother wavelet is chosen according to the signal and noise characteristics.
- Level is defined up till which the original signal is decomposed into approximation and detail coefficients.
- The components corresponding to PD or arcing signals, interference, and random noise are identified at each level by inspection and knowledge of frequency characteristics.
- Components corresponding to interference and random noise are discarded.
- De-noised signal is composed of cutting the low level noises in the useful signals by thresholding and by adding up all the useful signals.
- One of the common techniques to select components for reconstruction is the dominant frequency and amplitude.

The selection of “mother wavelet” is an important consideration in the above procedure. The mother wavelet, having the closest resemblance to the original signal, is preferred for de-noising. Among the wavelets available, the Daubechies wavelet family has almost all the required properties such as compactness, limited duration, orthogonal and asymmetric for analysis of fast transient and irregular PD pulses [28], [29]. Therefore, it is selected to de-noise PD and arcing measurements in this work. Dominant frequency is defined as the frequency content in the signal with highest amplitude. It can be determined using fast Fourier Transform (FFT) analysis. The dominant frequency and pre-defined mother wavelet along with the sampling frequency, determine the number of levels up to which the signal must be decomposed through MSD. In manual de-noising procedure, number of levels is determined using hit and trial method without calculating the dominant frequency. However, an automated methodology to determine the number of levels for adaptive de-noising is presented in section V.

The reconstruction of the signal based on the selected components gives an interference-free signal. The dominant frequency and dominant amplitude criteria, to select components for reconstruction, is promising in the case when noise level is lower than PD level. However if noise level is higher, then other techniques mentioned in the second paragraph of section III (C) can be combined with DWT.

The analysis and synthesis in multi-resolution signal decomposition (MSD) in DWT is depicted in Fig. 8. In this Figure “ $X[n]$ ” is the signal to be de-noised. Signal is split up into high frequency and low frequency component by filters (H_0 and G_0), followed by down sampling and so detail coefficients (high frequency) and approximation coefficients (low frequency) are achieved. In Fig. 8, $d_1[n]$, $d_2[n]$ and $d_3[n]$ are the detail coefficients at level 1, 2 and 3 respectively whereas $a_3[n]$ is the approximation at level 3.

B. De-Noising of Laboratory Measured Signals

Following signals have been used for de-noising. The two signals have sampling frequencies of 2 GS/s and 20GS/s respectively. PD signals are very small in magnitude (few mV) and hence more affected by the external noise whereas the arcing signals have relatively higher energy. So, de-noising

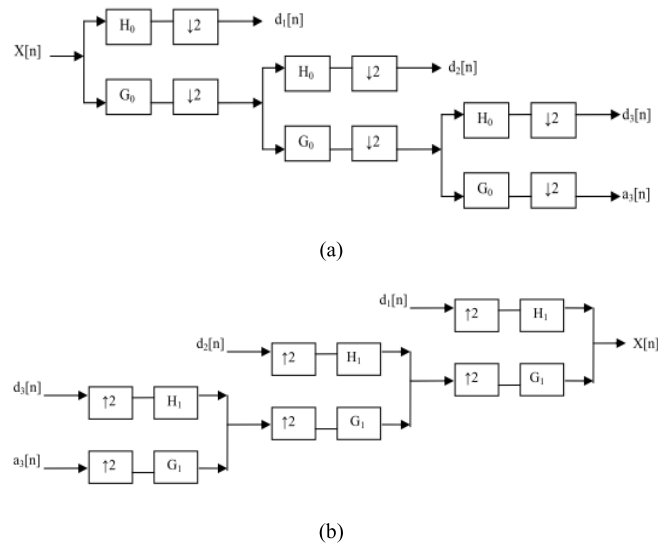


Fig. 8. (a) Multi-resolution signal decomposition in DWT. (b) Reconstruction.

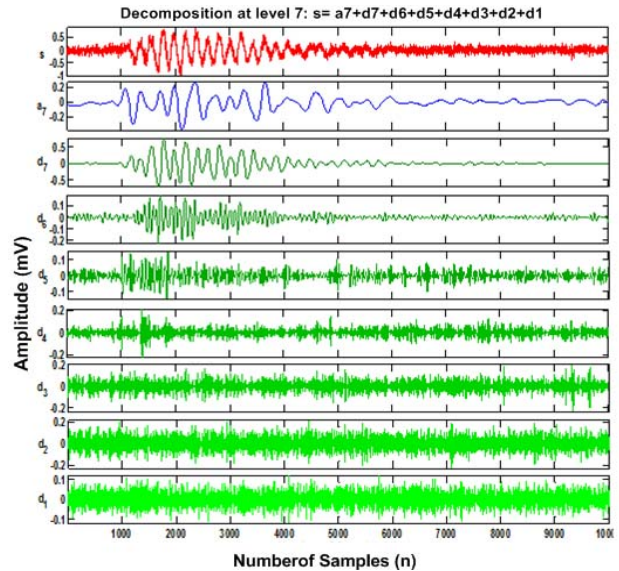


Fig. 9. Decomposition and approximation coefficients of Signal-1: (bottom to top) d_1 - d_7 , a_7 , s (original signal).

of PD signals is more necessary as compared to the arcing signals.

- **Signal-1:** PD signal captured by *D*-dot sensor.
- **Signal-2:** Arcing signal captured by *D*-dot Sensor.

For the processing of signal-1 using MSD, signal is decomposed up to level 7 using “Daubechies-7” as a mother wavelet. Fig. 9 shows the detail components (d_1 - d_7), approximation (a_7) of the signal-1 (s). As it is explained in section IV (A), the useful detail components are identified on the basis of their amplitudes compared to the original signal (to be de-noised), wave shape and dominant frequency. Figure shows that only d_7 matches in wave shape and amplitude with the original signal. Therefore, the de-noised signal is obtained by selecting the detail component at level 7 (d_7) only and all other

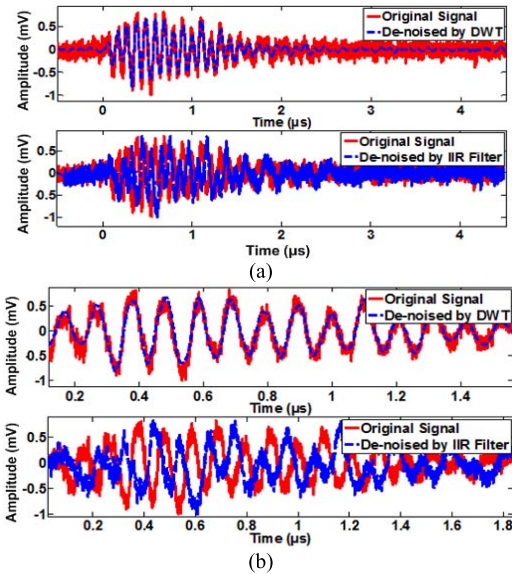


Fig. 10. Time domain comparisons of Signal-1. (a) (top) Original signal versus de-noised signal by DWT and (bottom) original signal versus de-noised signal by IIR filter. (b) Zoomed version of (a).

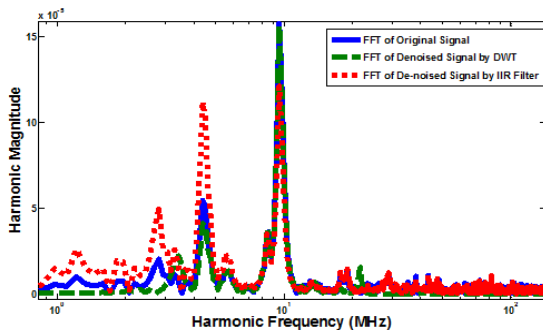


Fig. 11. Frequency domain comparison between original and de-noised signals (Signal-1).

detail components are discarded. The discarded components can be clearly seen as high frequency white noise (d_1 - d_5), high frequency resonance caused by reflections (d_6) and low frequency resonance (a_7) having very low amplitude and not clearly visible in the original signal either. The thresholding technique is used to eliminate low level noise superimposed on the useful signal in an individual detail component. As it is clear from Fig. 9, the selected useful component (d_7) contains negligible level of noise, therefore, thresholding is not used for this signal. Due to the same reasons, it is not used in this paper because of the presence of low level noise in the useful decomposed components. The original and de-noised signals are plotted on the same time scale in Fig. 10, whereas Fig. 11 shows the frequency domain comparison between them. For comparison an IIR band-pass filter (Butterworth type) of order 10 having frequency band from 1-12 MHz is applied for noise elimination. Figures 10 (a)-top and (a)-bottom show the de-noised signal by DWT and IIR filter respectively. Fig. 10(b) shows the zoomed version of (a).

Fig. 11 shows the comparison between FFT of original and de-noised signals. Pulse shape of the de-noised signals by IIR has been deformed which is clear from the change

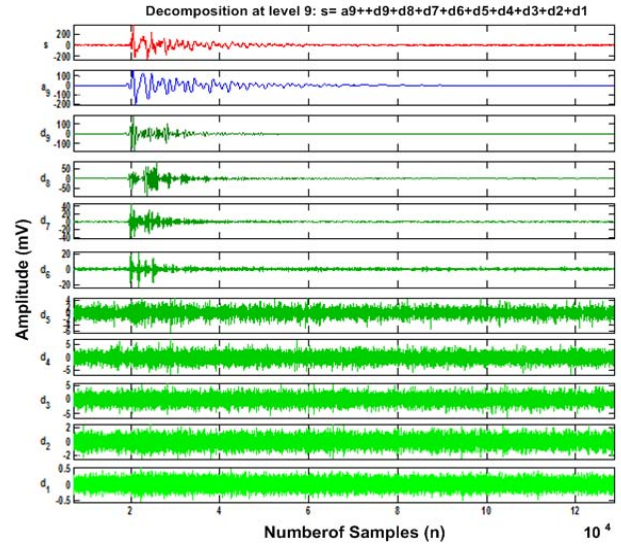


Fig. 12. Decomposition and approximation coefficients of Signal-2: (bottom to top) d_1 - d_9 , a_9 , s (original signal).

in dominant frequency spectrum. Whereas FFT of DWT de-noised signal is much closer to the original signal at dominant frequencies and has removed high frequency contents. Comparisons confirm that the DWT technique has successfully de-noised actual PD signal from high frequency interferences, electric and magnetic field coupling and reflections in the measurement system. In order to get clear idea about the nature of fault, it is recommended to perform such de-noising techniques before analysing signals and finding out fault features. As compared to the IIR filter technique, DWT is more efficient and helps to obtain better recovery of pulse shape, and a fine frequency separation.

For the processing of signal-2 that is due to an arcing event, it is decomposed up to level 9 using “Daubechies-7” as a mother wavelet. Fig. 12 shows the detail components (d_1 - d_9) and approximation (a_9) of the signal-1 (s). The de-noised signal is obtained by selecting the detail component at level 9 (d_9) and approximation (a_9) i.e. $d_9 + a_9$, due to their comparable amplitudes and wave shapes with the original signal, and all other detail components are discarded. The discarded components can be clearly seen as high frequency white noise (d_1 - d_5) and high frequency resonance caused by reflections (d_6 - d_8), having very low amplitude and not clearly visible in the original signal either. Figs. 13 and 14 show the time domain and frequency domain comparisons between original and de-noised signals. An IIR band-pass filter (Butterworth type) of order 10 having frequency band from 1-25 MHz is applied for noise elimination. Due to the lesser noise content in arcing signal as compared to PD signal, the arcing signals de-noised by the two techniques (DWT and IIR) are not much different. However, it is clear from Fig. 14 that high frequency noise (above 25 MHz) has been clearly removed by DWT, whereas IIR couldn't remove this noise.

C. De-Noising of Modelled Signal With On-Site Disturbances

The on-site monitoring has the major problem of electromagnetic interference (EMI) which often subsumes

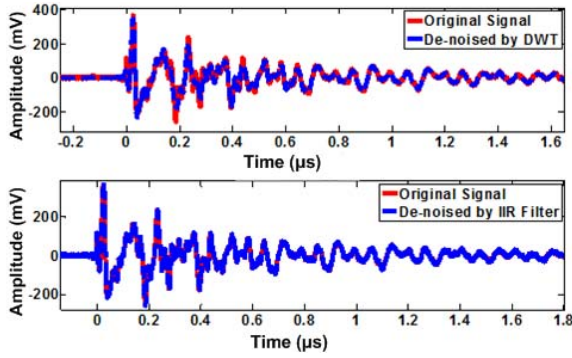


Fig. 13. Time domain comparisons of Signal-2. (top) Original signal versus de-noised by DWT. (bottom) Original signal versus de-noised by IIR filter.

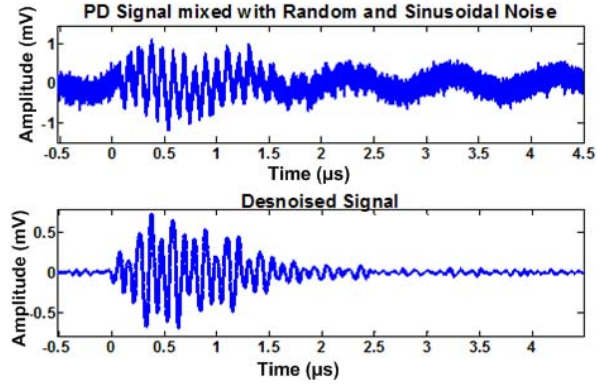


Fig. 15. De-noising of Signal-3. (top) Original signal. (bottom) De-noised by DWT.

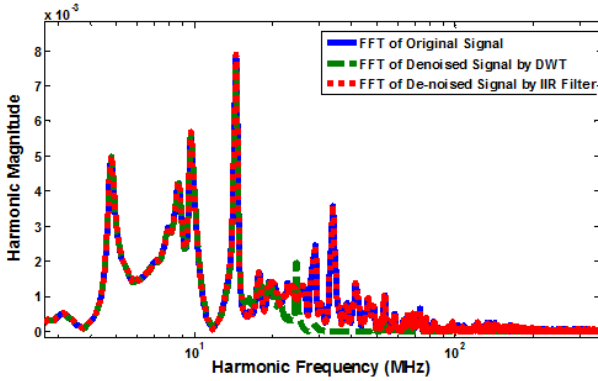


Fig. 14. Frequency domain comparison between original and de-noised signals (Signal-2).

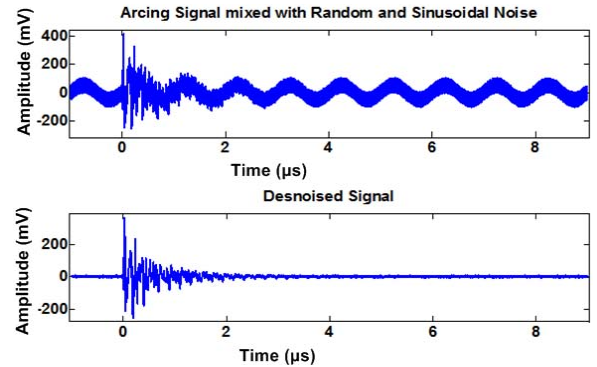


Fig. 16. De-noising of Signal-4. (top) Original signal. (bottom) De-noised by DWT.

completely the very low level discharge signals picked up by an unconventional sensor. For the processing of on-site measurements, signals captured in the laboratory setups have been mixed with different types of simulated disturbances in the following patterns:

- **Signal-3:** Signal-1 mixed with random noise and sinusoidal noise having frequency of 1 MHz.
- **Signal-4:** Signal-2 mixed with random noise and sinusoidal noise having frequency of 1 MHz.

For the processing of signal-3 using DWT technique, it is decomposed up to level 9 using “Daubechies-7” as a mother wavelet. The added random noise or white noise goes to high frequency decomposition components (from d_1 to d_4), similar to shown in Fig. 9. The selection of useful signals for reconstruction is same as signal-1 and signal-2 but additionally the sustained sinusoidal noise is also eliminated, which lies at approximation coefficient. The de-noised signal is obtained by selecting the detail components at level 7 only and the rest are discarded. The actual and the de-noised signal-3 are shown in Fig. 15. It is clear that WT technique has de-noised PD signal mixed with random noise and sinusoidal noise of 1 MHz. If we compare the pulse shape of the de-noised signal with Signal-1, it is almost the same. This proves the effectiveness of the technique for on-site measurements too. In order to process signal-4 using MSD, “Daubechies-7” is used as a mother wavelet and signal-4 is decomposed up to level 12. The de-noised signal is obtained by selecting the

detail components at level 9, 10 and 11 only and the rest are discarded. The actual and the de-noised signal-4 are shown in Fig. 16.

In the above cases, a single radio frequency interference (1MHz) is taken into account for DSI as an example and to keep the case simple. However, various AM/FM radio frequencies interferences with PD measurements are possible in the real on-site environment. The more practical situation can be simulated by mixing random noise with various combinations of AM/FM frequencies in the measured PD signal and applying de-noising technique. During the processing of above mentioned signals, the minimum loss of pulse magnitude and distortion of pulse shape is obtained using DWT technique, which is a significant consideration for online PD measurements and further quantification of the measured results.

V. ADAPTIVE DE-NOISING APPROACH

Previous section explains the de-noising of laboratory measurements which are already saved on computing or processing device and de-noising is done manually by using Matlab program. In this section, programming of signal processing unit is explained in order to achieve adaptive de-noising without human intervention, as shown in Fig. 17.

After the data acquisition, amplitude of the captured signal is calculated on the basis of peak to peak value or maximum value in terms of volts or milli-volts. FFT of the signal is

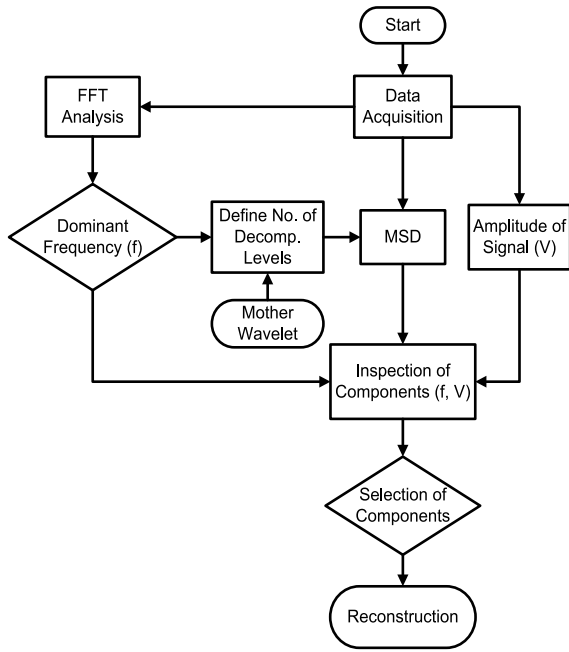


Fig. 17. Flow chart of adaptive de-noising procedure.

calculated in order to find the dominant frequency component of the signal. A suitable mother wavelet is preset. For PD and arcing signals, Daubechies mother wavelet gives satisfactory results [28].

Dominant frequency and pre-defined mother wavelet along with the sampling frequency, determine the number of levels up to which the signal must be decomposed through MSD. Frequency spectrum of each decomposition level for a certain mother wavelet at a given sampling rate is defined by the low pass and high pass filters of a mother wavelet. Number of levels is selected in such a way that dominant frequency of the captured signal is contained within the decomposed coefficients. Once, signal is decomposed into different decomposition coefficients and approximation, their amplitudes are compared with the amplitude of the captured signal. The components having frequency spectra in the range of dominant frequency and amplitudes comparable with the captured signals are selected. Rests of the components are discarded. Mostly present AM and FM radio frequency signals are also discarded. Finally de-noised signal is reconstructed by adding up selected signals.

In order to have better understanding of the above methodology, de-noising of Signal-1 (already de-noised in the previous section) can be explained with respect to this approach. If signal was captured online, FFT could indicate that dominant frequency is at 10 MHz. For a signal having 2GS/s sampling rate, by selecting Daubechies-7 as mother wavelet, 10 MHz signal is expected at decomposition level 7. Hence minimum of 7 levels are selected for MSD. After MSD, frequency spectrum of each component is compared with the dominant frequency. Also the peak to peak values are compared with the peak to peak values of the captured signal. During this analysis, decomposition coefficient at level 7 (i.e. d_7) turns out to be the de-noised signal.

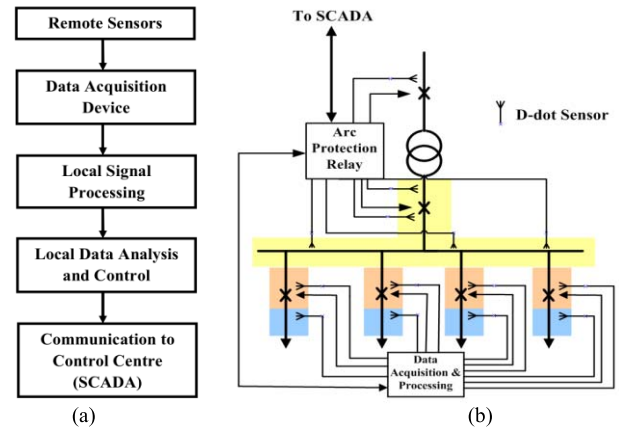


Fig. 18. Online monitoring system. (a) Flow chart of online monitoring. (b) Typical implementation in MV substation.

VI. ONLINE MONITORING AND PRO-ACTIVE DETECTION

Fig. 18 shows a possible implementation of online monitoring system in a typical MV distribution system where D -dot sensors are installed near breaker poles, in the bus-bar compartment and in the outgoing cable termination boxes. One sensor in each section of switchgear is sufficient for PD or arcing detection. The essential purpose of online monitoring of switchgear is to prevent high energy faults. An online monitoring system should be able to analyze the measured data, and provide appropriate information to upper level systems, such as protection system, programmable logic control (PLC) system, distributed control system (DCS) or supervisory control and data acquisition (SCADA) system.

Based on the importance of signal processing requirement presented in this paper, it is justified to have a separate processing unit, collecting information from the sensors, and sending the processed (de-noised) data to either remote systems (local data analysis and control centre) or to central control station (e.g through SCADA). Remote or local system (relays) may have a decision capability to decide about sending a trip signal directly to a circuit breaker before sending the information to the upper level, in order to avoid severe damage. This may happen in case of sudden faults. The presence of local control makes the system faster as compared to central control only. It also reduces the amount of data transmitted to SCADA. The data sent to the central control can be used for monitoring and efficient asset management purpose. The information to be sent to SCADA, can be an analog signal, indicating e.g. the level of PD activity, or it can be a digital information as well, e.g. alarms signal. An alarm signal can be an early warning, giving opportunity to check other possible indications of developing fault, and change power system switching state to isolate the zone of the developing fault.

VII. CONCLUSION

Two major types of slowly developing faults that lead to high energy arc faults in a switchgear, are bad contacts and insulation degradation. These faults are sources of transients and PDs in MV switchgear. A differential electric field sensor (D -dot) has been proposed for online monitoring of air

insulated switchgear. It is a unique application of this sensor. The sensor is recommended due to its low cost, smaller size, simple design and easy implementation as compared to other sensors. Its sensitivity and performance comparison with HFCT proves its reliability for online monitoring of switchgear.

On-site measurements of such transients are strongly influenced by external interference or noise. DWT technique is used in this paper to de-noise PD signals and arcing transients, affected by external noise and captured by the *D*-dot sensor. DWT is based on multi-resolution signal analysis both in time and frequency domain. The de-noising procedure has been discussed in detail. The captured signals are also mixed with simulated noise (random and sinusoidal) and then de-noised using this technique. Comparison carried out between the original and the de-noised signals both in time and frequency domains clearly show the significance of DWT over IIR filtering technique to de-noise PDs and low power arcing signals.

The sensor and signal processing can be integrated in distribution automation. A dedicated data acquisition and processing device is recommended for the arc protection. The output from the device can be integrated into the protection relays and distribution automation system. The implementation of this technology in industry may provide promising results in avoiding arc flashes in the switchgear.

ACKNOWLEDGMENT

The authors highly appreciate the valuable and interesting discussions with Joni V. Klüss (Aalto University, School of Electrical Engg., Espoo, Finland) and Dr. Nagy I. Elkalashy (Dept. of Electrical Eng., Minoufiya University, Egypt).

REFERENCES

- [1] G. A. Hussain, "Methods for arc-flash prediction in MV/LV switchgear," M.S. thesis, School Elect. Eng., Aalto Univ., Espoo, Finland, Nov. 2011.
- [2] H. B. Land, C. L. Eddins, L. R. Gauthier, Jr., and J. M. Klimek, "Design of a sensor to predict arcing faults in nuclear switchgear," *IEEE Trans. Nucl. Sci.*, vol. 50, no. 4, pp. 1161–1165, Aug. 2003.
- [3] D. Brechtken, "Preventive Arc Fault Protection," in *Proc. IEEE/PES Transmiss. Distrib. Conf. Expo.*, Oct./Nov. 2001, pp. 311–316.
- [4] L. Kumpulainen, G. A. Hussain, M. Lehtonen, and J. A. Kay, "Pre-emptive arc fault detection techniques in switchgear and controlgear," *IEEE Trans. Ind. Appl.*, vol. 49, no. 4, pp. 1911–1919, Jul./Aug. 2013.
- [5] J. A. Kay, J. Arvola, and L. Kumpulainen, "Protecting at the speed of light," *IEEE Ind. Appl. Mag.*, vol. 17, no. 3, pp. 12–18, May/June 2011.
- [6] T. R. Dugan, "Reducing the arc flash hazard," *IEEE Ind. Appl. Mag.*, vol. 13, no. 3, pp. 51–58, May/June 2007.
- [7] C. Sumereder and M. Muhr, "Estimation of residual lifetime—Theory and practical problems," in *Proc. 8th Höfler's Days*, Portoroz, Slovenia, Nov. 2005, pp. 1–6.
- [8] F. Senn, M. Muhr, W. Ladstätter, and W. Grubelnik, "Complexity of determining factors for the thermal evaluation of high voltage insulation systems on the example of rotating machines," in *Proc. DISEE*, Demänovská Dolina, Slovakia, 2008, pp. 1–4.
- [9] J. V. Klüss, "Measuring picosecond flashover in pressurized sulfur hexafluoride (SF₆)," M.S. thesis, School Elect. Eng., Aalto Univ., Espoo, Finland, 2011.
- [10] M. Aro, J. Elovaara, M. Karttunen, K. Nousiainen, and V. Palva, *Suurjännitetekniikka*, 2nd ed. Helsinki, Finland: Otatieto, 2003.
- [11] S. Xiao, P. J. Moore, M. D. Judd, and I. E. Portugues, "An investigation into electromagnetic radiation due to partial discharges in high voltage equipment," in *Proc. IEEE Power Eng. Soc. General Meeting*, Jun. 2007, pp. 1–7.
- [12] M. Muhr, *Non-Conventional PD Measurements*, document IEC TC42 WG14, 2012.
- [13] M. A. Stuchly and S. S. Stuchly, "Coaxial line reflection methods for measuring dielectric properties of biological substances at radio and microwave frequencies—A review," *IEEE Trans. Instrum. Meas.*, vol. 29, no. 3, pp. 176–183, Sep. 1980.
- [14] G. B. Gajda and S. S. Stuchly, "Numerical analysis of open-ended coaxial lines," *IEEE Trans. Microw. Theory Techn.*, vol. 31, no. 5, pp. 380–384, May 1983.
- [15] S. Burkhart, "Coaxial E-field probe for high-power microwave measurement (short papers)," *IEEE Trans. Microw. Theory Techn.*, vol. 33, no. 3, pp. 262–265, Mar. 1985.
- [16] T. P. Budka, S. D. Waclawik, and G. M. Rebeiz, "A coaxial 0.5–18 GHz near electric field measurement system for planar microwave circuits using integrated probes," *IEEE Trans. Microw. Theory Techn.*, vol. 44, no. 12, pp. 2174–2184, Dec. 1996.
- [17] Y. Gao and I. Wolff, "A simple electric near field probe for microwave circuit diagnostics," in *IEEE MTT-S Int. Microw. Symp. Dig.*, vol. 3, Jun. 1996, pp. 1537–1540.
- [18] J. R. Andrews, "UWB signal sources, antennas & propagation," Picosecond Pulse Labs, Boulder, CO, USA, Appl. Note AN-14a, 2003.
- [19] I. A. Metwally, "*D*-Dot probe for fast-front high-voltage measurement," *IEEE Trans. Instrum. Meas.*, vol. 59, no. 8, pp. 2211–2219, Aug. 2010.
- [20] J. V. Klüss and P. Hyvönen, "Empirical analysis of picosecond breakdown in sulfur hexafluoride," *J. Electrostatics*, vol. 71, no. 4, pp. 603–610, Aug. 2013.
- [21] J. V. Klüss and P. Hyvönen, "Practical e-field sensors for EMP testing," in *Proc. Int. Conf. High Voltage Eng. Appl. (ICHVE)*, Sep. 2014, pp. 1–4.
- [22] Y. Wang, J. Li, and L.-X. Ran, "An equivalent circuit modeling method for ultra-wideband antennas," *Prog. Electromagn. Res.*, vol. 82, no. 4, pp. 433–445, 2008.
- [23] M. Shafiq, L. Kutt, M. Lehtonen, T. Nieminen, and M. Hashmi, "Parameters identification and modeling of high-frequency current transducer for partial discharge measurements," *IEEE Sensors J.*, vol. 13, no. 3, pp. 1081–1091, Mar. 2013.
- [24] G. C. Stone, "Partial discharge diagnostics and electrical equipment insulation condition assessment," *IEEE Trans. Dielectr. Electr. Insul.*, vol. 12, no. 5, pp. 891–904, Oct. 2005.
- [25] M. Hikita, S. Okabe, H. Murase, and H. Okubo, "Cross-equipment evaluation of partial discharge measurement and diagnosis techniques in electric power apparatus for transmission and distribution," *IEEE Trans. Dielectr. Electr. Insul.*, vol. 15, no. 2, pp. 505–518, Apr. 2008.
- [26] G. A. Hussain, L. Kumpulainen, J. V. Klüss, M. Lehtonen, and J. A. Kay, "The smart solution for the prediction of slowly developing electrical faults in MV switchgear using partial discharge measurements," *IEEE Trans. Power Del.*, vol. 28, no. 4, pp. 2309–2316, Oct. 2013.
- [27] V. Nagesh and B. I. Gururaj, "Evaluation of digital filters for rejecting discrete spectral interference in on-site PD measurements," *IEEE Trans. Electr. Insul.*, vol. 28, no. 1, pp. 73–85, Feb. 1993.
- [28] M. Hashmi, M. Lehtonen, M. Nordman, R. A. Jabbar, and S. A. Qureshi, "Wavelet-based de-noising of on-line PD signals captured by Pearson coil in covered-conductor overhead distribution networks," *Int. J. Elect. Power Energy Syst.*, vol. 43, no. 1, pp. 1185–1192, Dec. 2012.
- [29] L. Satish and B. Nazneen, "Wavelet-based denoising of partial discharge signals buried in excessive noise and interference," *IEEE Trans. Dielectr. Electr. Insul.*, vol. 10, no. 2, pp. 354–367, Apr. 2003.
- [30] C. S. Burrus, R. A. Gopinath, and H. Guo, *Introduction to Wavelets and Wavelet Transforms: A Primer*. Upper Saddle River, NJ, USA: Prentice-Hall, 1998.



Ghulam Amjad Hussain (S'06–M'06) is pursuing the Ph.D. degree in electrical engineering (power systems and high voltage) from Aalto University, School of Electrical Engineering, Finland. He received the bachelor's degree in electrical engineering from the University of Engineering and Technology, Lahore, Pakistan, in 2007, and the master's degree from Aalto University, School of Electrical Engineering, Finland, in 2012. He has published more than 25 articles in highly reputed international journals and conferences. His fields of interest are pre-emptive protection techniques and on-line condition monitoring of electrical substation and network.



Muhammad Shafiq received the Ph.D. degree in electrical engineering (power systems and high voltage engineering) from Aalto University, School of Electrical Engineering, Finland, in 2015, and the B.Sc. and M.Sc. degree in electrical engineering from the University of Engineering and Technology (UET), Lahore, Pakistan, in 2001 and 2007, respectively. He had been working as an Assistant Professor at Engineering College IUB Pakistan during 2002-2009. He has published more than 35 articles in highly reputed international journals and conferences. His fields of interest are pre-emptive protection techniques and on-line condition monitoring of electrical substation and network.



Matti Lehtonen (M'12) received the M.Sc. and Licentiate degrees in electrical engineering from the Helsinki University of Technology, Espoo, Finland, in 1984 and 1989, respectively, and the Dr.Tech. degree from the Tampere University of Technology, Tampere, Finland, in 1992.

Since 1987, he has been with the Technical Research Centre of Finland, Espoo, Finland, and Aalto University, Espoo, Finland, since 1999, where he is a Professor of Power Systems, High Voltage and IT Applications in Power Systems. He has authored many conference and journal papers.



Murtaza Hashmi received B.Sc. degree in electrical engineering from the University of Engineering and Technology (UET), Lahore, Pakistan, the M.S. degree in electrical engineering from the Royal Institute of Technology (KTH) Stockholm, Sweden, and the D.Sc. Tech. degree from the Helsinki University of Technology (TKK) Espoo, Finland, in 1994, 2001, and 2008, respectively. Since 1995, he worked as a Facilities Engineer with Pakistan State Oil Co. Ltd. From 2001 to 2004, he was an Associate Professor with the Electrical Engineering Department, UET. Since 2007, he worked as a Power Distribution Specialist at ABB Finland. From 2010 to 2013, he was a Senior Scientist with Energy Systems Knowledge Centre at VTT Technical Research Centre of Finland. Currently, he is working as a Condition Monitoring Expert with the Power Systems Engineering Department. His major interests are condition monitoring and asset management of power systems, partial discharge detection for diagnostics and fault location and smart grids. He has published more than 50 articles in reputed refereed international journals and conferences. He is member of PEC and GCC CIGRE.